Acta Cryst. (1995). A51, 391–398

Reflectivity Curves of Bragg Reflections from Small Imperfect Single Crystals

BY A. MCL. MATHIESON

Chemistry Department, La Trobe University, Bundoora, Victoria 3083, *Australia, and Division of Materials Science and Technology, CSIRO, Private Bag* 33, *Rosebank MDC, Clayton, Victoria* 3169, *Australia*

AND A. W. STEVENSON

Division of Materials Science and Technology, CSIRO, Private Bag 33, *Rosebank MDC, Clayton, Victoria* 3169, *Australia*

(*Received* 3 *June* 1994; *accepted* 19 *December* 1994)

Abstract

A slice-scan procedure involving a narrow aperture in front of the detector can allow determination of the extinction-affected reflectivity curve, $r^*(\Delta\omega)$, of Bragg reflections from a small imperfect single crystal. The measured curve can be corrected for the effect of the remaining truncated components, associated with the source emissivity and wavelength distributions which are passed by the narrow aperture. Because of the small area of diffraction space associated with this procedure compared with that for the conventional wide-aperture reflection profile, contributions from TDS, air scatter and incoherent radiation are greatly reduced. By the very nature of reflectivity curves, their determination does not involve a systematically increasing $\Delta\omega$ angular range dependent on $\tan\theta$.

1. Introduction

Only on rare occasions has an attempt been made to establish experimentally the reflectivity distributions of Bragg reflections from imperfect crystals, *e.g.* Robinson (1933) and Schneider (1977). Generally, the attainment of reflectivity distributions has neither been perceived as feasible, except under special conditions, nor indeed as warranting the necessary effort.

The reflectivity distribution has, however, certain advantages over the conventional reflection profile. Since it is a one-dimensional distribution of varying reflectivity, it has the potential for correction point by point for the effect of secondary extinction,† see Robinson (1933) and Schneider (1977). The reflectivity distribution is, of course, the fundamental distribution whose integration leads to an estimate of the structure factor. If corrected appropriately, it can provide an estimate that is extinction free.

† The conventional procedure in relation to extinction is to deduce, from a theoretical model, single-valued (average) correction in relation to the 'integrated intensity' of the reflection profile, see *e.g. International Tables for Crystallography* (1992).

Our studies in two-dimensional $\Delta\omega, \Delta 2\theta$ diffraction space, see Mathieson (1982, 1984, 1985) and Mathieson & Stevenson (1984, 1986*a*,*b*, 1993), have led to an appreciation of how to select a very restricted slice of diffraction space and hence determine, in a relatively simple experimental manner, the intrinsic one-dimensional extinction-affected reflectivity distribution of Bragg reflections of small imperfect single crystals.

2. The relation of the reflectivity distribution and the reflection profile

To avoid ambiguity in our subsequent discussion, certain terms are defined here. The one-dimensional reflectivity distribution, $r(\Delta\omega)$ [or rather the extinguished reflectivity distribution, $r^*(\Delta\omega)$], for a point imperfect crystal is defined as the ratio of the intrinsic diffracted intensity at the crystal setting angle, $\Delta\omega$, to the incident intensity, associated with a vanishingly small source of radiation emitting a single δ-function wavelength. The one-dimensional reflection profile, $I(\Delta\omega)$, corresponds to the interaction of the reflectivity distribution with a source of significant size and with its natural wavelength distribution and a crystal of particular shape and size (bathed within the beam), the diffracted beam being passed by a wide detector aperture (other possible additional components may have to be taken into account in specific cases). It is the reflection profile that corresponds to the conventional measurement. A slice scan (Mathieson, 1982) corresponds to a scan procedure, ω, ω/θ, $\omega/2\theta$ or 2θ (Furnas, 1957), where the aperture in front of the detector is narrow, *e.g.* 50–100 μm. The resolution function for a diffractometer is a result of the interaction of the various components, such as the emissivity distribution and wavelength distribution of the source, the size of the detector aperture, and the size (shape) of the specimen crystal but excluding the crystal imperfections, *cf.* Mathieson & Stevenson (1993).

For our purposes, it is instructive to synthesize, step by step, a conventional one-dimensional $I(\Delta\omega)$ reflection profile in relation to its usual main components.

The components that we will progressively introduce in modelling the profile of a reflection at $\theta = 20°$ are the extinguished reflectivity distribution, $r^*(\Delta\omega)$, represented as a Gaussian of FWHM of 0.04°, a source emissivity distribution, σ, corresponding to a trapezoid of base width 0.153° and width at the top 0.092° (equivalent to an effective source of width 0.8 mm 300 mm from the crystal), and a wavelength distribution, λ, consisting of two Lorentzians equivalent to Mo $K\alpha$ radiation for a reflection of $\theta = 20°$. These are shown in Fig. 1 in respect of their $\Delta\omega$ variable. The $\Delta\omega, \Delta 2\theta$ distributions have been calculated using cross multiplication and convolution in two dimensions; see Mathieson & Stevenson (1993) for the justification for these individual procedures.

Consider the situation of diffraction from a point imperfect crystal with the nominated reflectivity distribution in relation to two-dimensional $\Delta\omega, \Delta 2\theta$ space, with a vanishingly small source of X-rays whose emissivity is limited to one wavelength (a δ function). Fig. 2(*a*)(i) shows the locus of the diffracted signal in $\Delta\omega, \Delta 2\theta$ space for a reflection H. The intensity profile of the diffracted signal, projected along the $\Delta 2\theta$ axis, Fig. 2(*a*)(ii), yields the reflectivity distribution $r_H(\Delta\omega)$ or, more correctly, the extinction-affected reflectivity distribution $r_H^*(\Delta\omega)$ as in†

$$I_H(\Delta\omega) = r_H^*(\Delta\omega) I_0. \qquad (1)$$

Now introduce a source of conventional size (spot focus mode) while maintaining the δ-function wavelength distribution. The resultant combination of the r^* distribution with each point of the source distribution, σ, leads to the two-dimensional distribution lying within the parallelogram *ABCD* representing the effective outer limits of the interaction of the two functions [Fig. 2(*b*)(i)]. When integration parallel to the $\Delta 2\theta$ axis (equivalent to the normal use of a wide aperture in front of the detector) is carried out, it yields the profile on the right [Fig. 2(*b*)(ii)]. The r^* distribution has largely been masked, leaving the only evidence of its existence in respect of the edges of the profile.

† We take the view that, in principle, all reflections are affected by extinction other than those of zero intensity (Mathieson, 1979).

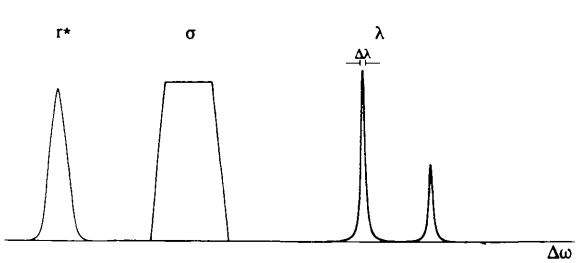

Fig. 1. The main components of a reflection profile, the extinguished reflectivity distribution, $r^*(\Delta\omega)$, the emissivity distribution, σ, and the wavelength distribution, λ, of the source, the last corresponding to Mo $K\alpha$ radiation and $\theta = 20°$.

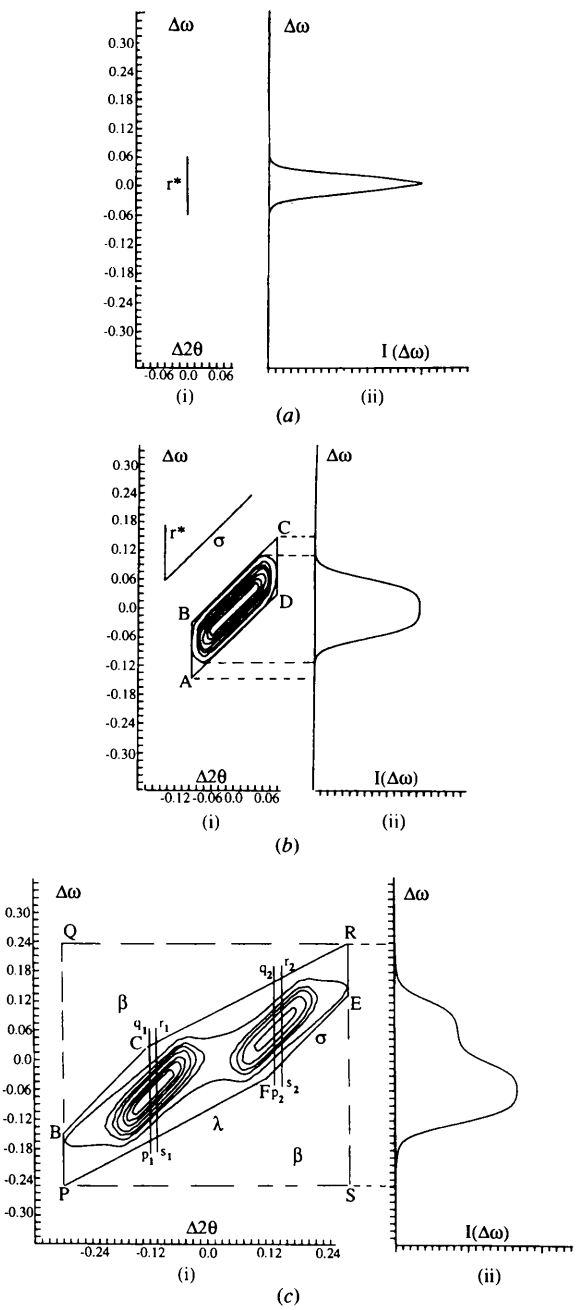

Fig. 2. (*a*)(i) The locus of the reflectivity distribution in $\Delta\omega, \Delta 2\theta$ diffraction space. (ii) The projected intensity distribution, $r^*(\Delta\omega)$. (*b*)(i) The two-dimensional distribution, in $\Delta\omega, \Delta 2\theta$ space, of the interaction of the r^* and σ distributions, lying within the outer-limit parallelogram, *ABCD*. The loci of r^* and σ are shown. (ii) The one-dimensional distribution, $I(\Delta\omega)$, resulting from projection of the 2D distribution along the $\Delta 2\theta$ axis. (*c*)(i) The two-dimensional distribution resulting from the interaction of the 2D distribution in (*b*)(i) with the λ distribution, lying within the outer-limit polygon, *PBCREF*. The area *PQRS* is that area of diffraction space that would be integrated if the detector aperture corresponded to *PS*. $p_1q_1r_1s_1$ represents the area of diffraction space associated with α_1 and intercepted by a slice scan using a narrow detector aperture of size p_1s_1. $p_2q_2r_2s_2$ is the corresponding area for α_2. (ii) The one-dimensional distribution, $I(\Delta\omega)$, resulting from projection of the 2D distribution along the 2θ axis.

Finally, introduce the wavelength distribution, λ. The interaction of this third component with all points of the parallelogram distribution in Fig. 2(*b*)(i) leads to the 2D distribution lying within *PBCREF* in Fig. 2(*c*)(i). Projection of this distribution parallel to $\Delta 2\theta$ yields the reflection profile in Fig. 2(*c*)(ii). The area to be integrated in relation to the three components is *PBCREF* but, since the detector aperture corresponds to *PS*, the (physical) integration with a diffractometer involves the area *PQRS*, which includes the additional areas in diffraction space designated β in Fig. 2(*c*)(i). The reflection profile has lost virtually all evidence of the reflectivity distribution and is now dominated by the wavelength and emissivity distributions. There would appear to be little hope of accurately regaining the original r^* distribution by mathematical manipulation of the profile, especially in any actual circumstance with the complication of 'noise'.

3. The $I_s(\Delta\omega)$ slice scan

Now consider the situation in Fig. 2(*c*)(i) if one limited oneself to the use of a narrow aperture in front of the detector, *i.e.* (say) p_1s_1, and recorded the distribution, $I_s(\Delta\omega)$, corresponding to the traverse of $\Delta\omega$. This picks out the emission mainly from the centre of the source and corresponds to a restricted part of the α_1 wavelength distribution. Effectively, in terms of $\Delta\omega$, $\Delta 2\theta$ space, the slice scan accepts the whole of the locus corresponding to the reflectivity signal, r^*, parallel to the $\Delta\omega$ axis, but severely cuts into the loci corresponding to the source emissivity, σ, and the wavelength distribution, λ. So the slice scan collects signal, $I_s(\Delta\omega)$, only from the area of diffraction space indicated by $p_1q_1r_1s_1$. This distribution is essentially indistinguishable from that in Fig. 2(*a*)(ii).

4. Extracting the reflectivity distribution, $r(\Delta\omega)$

Having shown how the slice scan is obtained, it is of interest to indicate how the slice-scan signal can be treated to obtain the reflectivity distribution. To demonstrate the capability of the procedure, a slightly more elaborate synthetic reflectivity distribution is invoked.

First, let us consider how the wavelength/source components contribute to the slice-scan distribution along $\Delta\omega$. This combination will be used to deconvolute the slice-scan distribution.

(i) *Wavelength/source components – the resolution function*

With a source that is of normal size and a wavelength distribution consisting of the two Lorentzians, equivalent to Mo $K\alpha$ and $\theta = 20°$, then the resultant $I(\Delta\omega, \Delta 2\theta)$ distribution is shown in Fig. 3(*a*)(i). The slice-scan distribution, $I_s(\Delta\omega)$, corresponding to an aperture width of $\Delta 2\theta = 0.02°$ (equivalent to an aperture of 100 μm at 300 mm from the crystal) is shown in Fig. 3(*a*)(ii). Along the slice scan, the distribution associated with the combination of the source and wavelength distributions is, owing to the slopes of their loci, limited in its angular range, in most cases, to half the source range. The dispersion of the combination is truncated by this limit. Hence, the wavelength dispersion in Fig. 3(*a*)(ii) corresponds to of the order of $\Delta\lambda/\lambda = 1.2 \times 10^{-3}$ (for $\theta = 20°$), see the $\Delta\lambda$ measure in Fig. 1. This is narrower than the α_1 component isolated (say) by use of a conventional monochromator crystal. Obviously, the smaller the source size, the narrower is the resultant wavelength dispersion.

This distribution in Fig. 3(*a*)(ii) can be designated the resolution function in respect of the slice scan in that it does not include the reflectivity distribution, see § 2.

(ii) *The reflectivity distribution*

Let the reflectivity distribution correspond to three fragments, each being a single Gaussian with FWHM of 0.03, 0.04 and 0.02° and peak height 0.7, 1.0 and 0.3, respectively, with relative positions as in Fig. 3(*b*)(i). The resultant $\Delta\omega, \Delta 2\theta$ distribution involving the three parameters r^*, σ and λ is shown in Fig. 3(*c*)(i) with the derived reflection profile being shown on the right in Fig. 3(*c*)(ii). The corresponding slice scan is shown in Fig. 3(*b*)(ii), the original reflectivity distribution being modified by convolution with the resolution function referred to above, the fragment on the right being enveloped by the central fragment. When the reverse operation of deconvolution with the resolution function is carried out, the result, Fig. 3(*b*)(iii), closely reproduces the original. The deconvolution was performed by inverting the appropriate Toeplitz matrix formed from the resolution function. Prior to matrix inversion, a singular value decomposition (SVD) was carried out, so that the condition number of the matrix could be determined and 'adjusted' as necessary.

(iii) *Questions of interference*

One can repeat the procedure with a slice scan using emission from the centre of the source but corresponding to the α_2 image, *cf.* $p_2q_2r_2s_2$ in Fig. 2(*c*)(i). Comparison of the two distributions, $I_s(\Delta\omega)\alpha_1$ and $I_s(\Delta\omega)\alpha_2$, allows a check for the possible effect of overlap from adjacent radiation tails. Thus, the distribution $I_s(\Delta\omega)\alpha_1$ will have no interference in its higher-angle range but may have some in the lower-angle range from the α_2 tail. For the distribution $I_s(\Delta\omega)\alpha_2$, the reverse will hold. They can therefore be compared to identify tail effects and, if necessary, a corrected distribution derived. To reduce possible interference, the selected points on the source images can be moved towards the low-2θ-angle side for α_1 and towards the high-angle side for α_2. Tactics of this type may be advisable when moving to reflections at lower θ values. If the two reflectivity curves

for α_1 and α_2 match satisfactorily, then they can be scaled and combined.

While $K\alpha$ radiation has value for internal comparisons of the responses to the two components, its doublet nature can cause problems, as noted above. For application of this slice-scan procedure, there is advantage in using singlet β radiation.

(iv) *Variation with* θ

With change of θ, the wavelength band for a set angular range of $\Delta 2\theta$ changes according to $(\tan\theta)^{-1}$ for any one λ component. Since the shape of the reflection distribution depends on convolution of the several components, its dependence on $\tan\theta$ is not a simple linear one, see Burbank (1964, footnote on p. 436). There are two possible ways of handling this situation. One could maintain the aperture size (= *ps*) adjusted very precisely to keep $\Delta\lambda$ constant. Since the source, in normal circumstances, is extended in $\Delta\omega, \Delta 2\theta$ space, the source component within the narrow aperture width is a square-topped distribution. The other possibility is to hold the detector aperture fixed and apply an appropriate correction factor to allow for the change in $\Delta\lambda$. This correction factor can be fairly readily calculated from the particular conditions of the experimental set-up ($\theta, \Delta 2\theta, \lambda$ distribution), *cf.* Fig. 3(*a*)(i). In respect of the operational λ distribution, care should be taken in its modelling, see Destro & Marsh (1993).

(v) *Crystal size*

An additional component in generating the total $\Delta\omega, \Delta 2\theta$ distribution is that associated with the size (shape) of the specimen crystal. Keulen (1969) has shown that the form (locus) of this component in $\Delta\omega, \Delta 2\theta$ space is two-dimensional – unlike those already dealt with which are one-dimensional. For a spherical crystal, with change of θ, the form rotates anticlockwise and changes its shape. Starting as a line at $\theta = 0°$, the locus first opens out, reaching an extended form at 45°, then contracts again to a line at $\theta = 90°$,

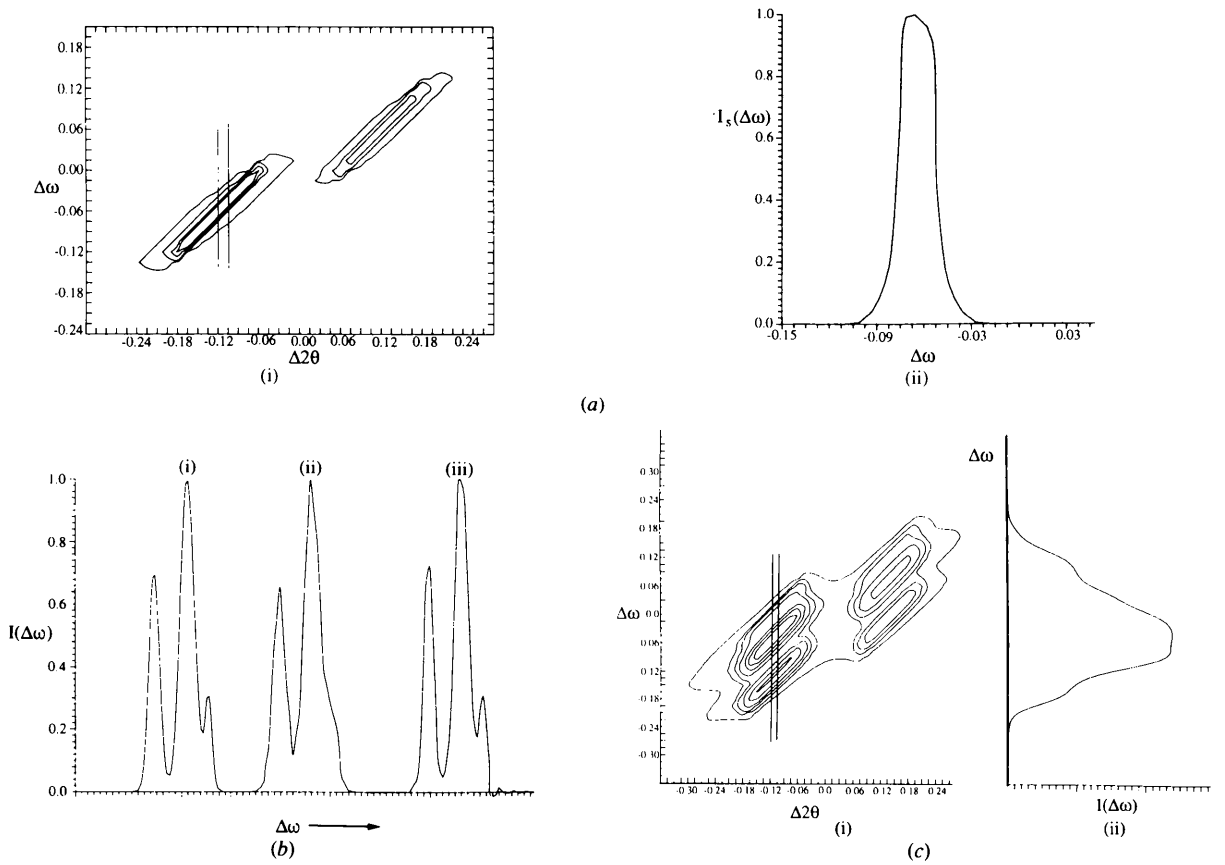

Fig. 3. (*a*)(i) The resolution function in $\Delta\omega, \Delta 2\theta$ space which involves the interaction of the emissivity distribution, σ, and the wavelength distribution, λ, of the source. The region of the slice scan, $I_s(\Delta\omega)$ is indicated. (ii) The slice-scan distribution, $I_s(\Delta\omega)$, through the centre of the α_1 image. (*b*)(i) A synthetic reflectivity distribution associated with three fragments, each a Gaussian, with peak heights 0.7, 1.0 and 0.3 and FWHM of 0.03, 0.04 and 0.02°, respectively. (ii) The slice scan, $I_s(\Delta\omega)$, through the centre of the α_1 image in (*c*)(i). (iii) The slice-scan distribution deconvoluted using the resolution function. (*c*)(i) The two-dimensional $\Delta\omega, \Delta 2\theta$ distribution resulting from the interaction of the three components, r, σ and λ. (ii) The projection of the 2D distribution to yield the reflection profile.

whose slope depends on the ratio of the source/crystal distance, δ_σ, to the crystal/detector distance, δ_τ. The outer $\Delta\omega$ and $\Delta 2\theta$ limits of the locus shape for $\delta_\sigma = \delta_\tau$ are as given in Mathieson (1984).

For $\theta = 20°$, the main axis of the locus shape lies between the λ locus and the σ locus, at a slope of ~0.57 to the $\Delta 2\theta$ axis. If its contribution in terms of $\Delta 2\theta$ is 0.02°, its contribution to the $\Delta\omega$ axis will be of the order of 0.011°. The combination of the truncated components for the source emissivity and wavelength distributions and the crystal size component passed by the aperture provides a function of FWHM of the order of 0.026°.

5. Absorption and extinction

The slice-scan procedure isolates the reflectivity curve, as affected by absorption and extinction, $r^*(\Delta\omega)$, *i.e.* the fundamental experimental evidence concerning the structure-factor value. The method discussed here does this with only minor involvement of the other components, exact knowledge of their magnitude therefore not being essential to the determination of the structure-factor value. By its very nature, the slice-scan procedure involves a minimal area of diffraction space, *i.e.* $p_1q_1r_1s_1$ *versus PQRS* for the normal wide-aperture procedure, see Fig. 2(*c*)(i). As a result, factors such as thermal diffuse scattering and general background due to air scatter and incoherently scattered radiation are greatly reduced. Correction by deconvolution of the measured reflectivity curve for the effect of the truncated source and truncated wavelength band is reasonably straightforward because these components are likely to be 'narrower' than a real reflectivity curve or at worst comparable.

Unlike reflection profiles, which, with increasing θ, are progressively dominated by the λ distribution, the reflectivity curves for a set of Bragg reflections will not expand significantly with increase in θ because the $\Delta\lambda$ band is very small. Indeed, with a detector aperture of constant size, the $\Delta\lambda$ band will contract with increase in θ. As a result, the setting of consistent outer limits of measurement (truncation limits) will be easier and intercomparison of reflections will be rendered more convenient. Thus, Fig. 4 shows (*a*) the slice scans of reflections 111, 333, 444 and 555 of a crystal of cubic BN compared with (*b*) the equivalent reflection profiles. If the 'mosaic spread' is isotropic, the reflectivity curves for all reflections will correspond to the same angular range. If there are variations in angular range, they will constitute evidence of anisotropic reflectivity and will be correlated with the inner morphology of the crystal, not with θ. These variations would require examination of measurements taken around the pole of the reflection, *cf.* Mathieson & Stevenson (1986*a*).

The capability of measuring a set of one-dimensional reflectivity curves, $r^*(\Delta\omega)$, for a group of Bragg reflections (and the potential for applying point-by-point corrections) opens up possibilities not previously available when one had only a set of single-valued quantities, corresponding to the integrated intensities.

As Robinson (1933) pointed out, in relation to his 001 reflection curves of anthracene crystals, the two main factors for which correction is required – absorption and (secondary) extinction – are path dependent. The correction for absorption, a purely volume effect independent of crystal orientation, can be readily calculated given the dimensional details of the specimen crystal (Robinson, 1933, and later references, *e.g.* in Clark, 1993), the same correction being applied to all parts of the reflectivity curve. The correction for secondary extinction varies with the magnitude of the reflectivity but use could be made of the absorption correction program in respect

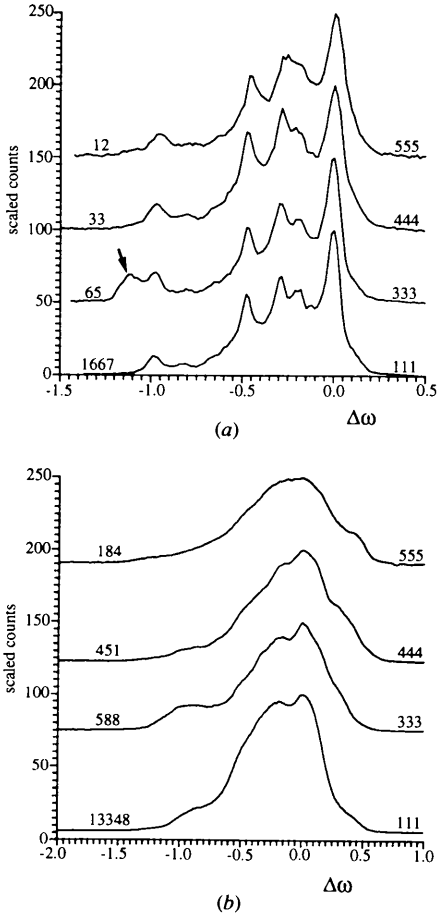

Fig. 4. Comparison of (*a*) the slice-scan distributions for the 111, 333, 444 and 555 reflections of a BN crystal with (*b*) the corresponding reflection profiles. The additional 511 component (due to twinning) occurring in the 333 slice scan is identified by an arrow. Figures on the left are proportional to the intensity of the main peak in each distribution; these correspond, in (*a*), to the centre of the $K\alpha_1$ distribution for all but the 111 curve (see text); for the 111 case, this was 1857. The actual 111 figure corresponds to a displacement to the left in the $K\alpha_1$ 'image' to reduce the effect of the $K\alpha_2$ wing. The curves are displaced vertically for clarity, the peak heights being normalized.

of path lengths for estimating extinction corrections, *cf.* Darwin's (1922) equations where absorption and scattering are both treated as path dependent. Robinson used crystal-monochromated radiation and made absolute estimates of reflection curves for one reflection, 001, of 18 crystals *versus* the intensity of the incident beam. As a result, he considered himself to be in a position to carry through a procedure to correct for extinction. The results were interesting but not decisive. The structure factor $F(001)$ with Cu $K\alpha$ radiation was 30.50 while that with Mo $K\alpha$ was 32.76. A subsequent estimate (Robinson, 1934) using powdered anthracene gave 34.30.

The correction for Cu was less successful than that for Mo but evidently the correction procedure was incomplete in both cases. From the current viewpoint, it is unlikely that Robinson's reflection profiles were true reflectivity distributions since his crystal monochromatization may have involved both α_1 and α_2. He noted (p. 440) in respect of a possible objection concerning beam divergence that 'This objection is immaterial, since we may regard each experimental curve obtained in divergent radiation as the result of superposing, with slight angular shifts, many curves each similar and belonging to some particular nearly parallel radiation beam'. In fact, the question of divergence is critical and the need for deconvolution of the experimental reflection profile with respect to both the source and wavelength distributions was only appreciated some time later (Stokes, 1948).

At the moment, there does not seem to be any obvious experimental procedure to put the slice-scan results on an absolute basis as Robinson did since one is using only part of the source and part of its wavelength distribution. However, where one is aiming to collect reflectivity data for a closer study of an already determined structure, one can visualize approaches based on approximate Q values allowing one to explore and extend Robinson's approach to correction for extinction. As he noted, the procedure, in principle, is capable of being iterative.

A possible problem in applying the slice-scan method is associated with crystals whose inner morphology is inhomogeneous, see Mathieson & Stevenson (1986*a*). It is therefore advisable to examine a few full-scale $\Delta\omega$, $\Delta 2\theta$ distributions from a specimen crystal to ensure that the crystal is suitable for the slice-scan procedure.

From a practical aspect, there would be an advantage in using a microfocus X-ray source of size (say) 50 μm or less where the specific intensity would be much enhanced relative to a more conventional source and, as pointed out earlier, the wavelength dispersion would be reduced.

6. Diffractometers with monochromators

It should be noted that, so far, discussion of this procedure has not made reference to monochromators. Where a monochromator crystal, M, is involved between the source and the specimen crystal, c, the situation depends on the orientation of the axis of M to that of c (case I in Mathieson, 1968). Where the axes are at right angles, *i.e.* $\varphi_M = 90°$ (or 270°), the wavelength dispersion of M is perpendicular to that of c so that they are effectively not coupled in the equatorial diffraction plane of c and the discussion in the main text is applicable to this monochromator configuration, *i.e.* to the majority of commercial laboratory instrument arrangements.

If, however, the axis of M is parallel to that of c, then, for the case of $\varphi_M = 180°$, *i.e.* the so-called parallel

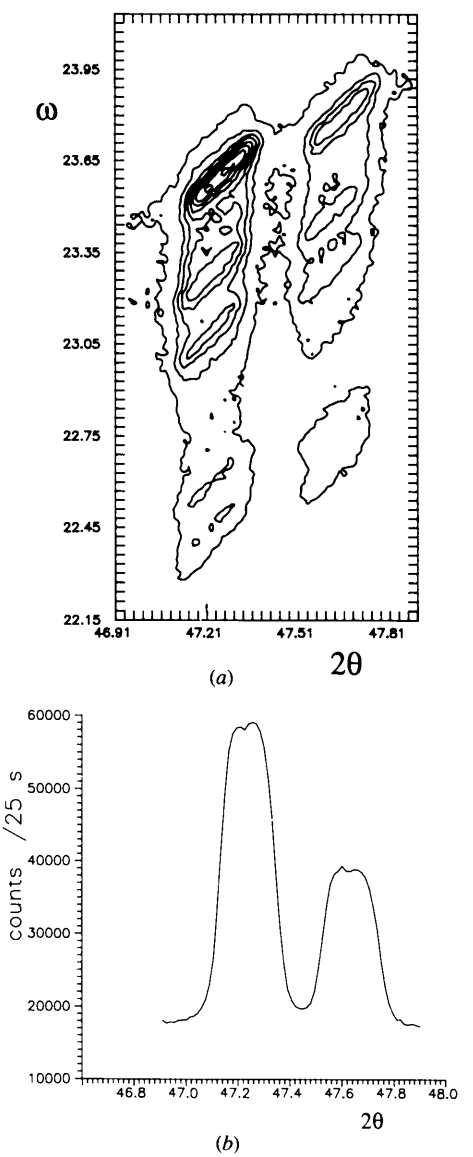

Fig. 5. (*a*) The $\Delta\omega$, $\Delta 2\theta$ distribution of the 333 reflection of the cubic BN crystal. (*b*) The corresponding 'film' profile, $I(\Delta 2\theta)$, derived by integration parallel to $\Delta\omega$. The structure seen at the top of each of the peaks in (*b*) we attribute to aspects of the source emissivity distribution. See also in (*a*).

region, the wavelength dispersion of M and c interact in such a way that the locus of the wavelength dispersion of the combination rotates in $\Delta\omega, \Delta 2\theta$ space as θ_c changes (Mathieson, 1985; Stevenson, 1989; Mathieson & Stevenson, 1993). Under these circumstances (which hold for most synchrotron facilities), care needs to be taken in the region of $t = \tan\theta_c/\tan\theta_M = 1/2$ when r^* and λ dispersion interact. In general, for the antiparallel region, $\varphi_M = 0°$, as well as the parallel region, the change of $\Delta\lambda$ with t has to be noted in calculating the resolution function.

7. Examples

Measurements to illustrate the procedure were made on two crystals, one of cubic BN and the other of magnetite. For BN, with a 'normal' source (size 0.8 mm) and Ag $K\alpha$ radiation, the $\Delta\omega, \Delta 2\theta$ distributions of 111 and 333 were recorded to establish that the crystal was fragmented but not distorted due to bending. For 111, the slice-scan $\Delta 2\theta$ setting in the $K\alpha_1$ region was selected to ensure no overlap with $K\alpha_2$. In the case of 333 and higher orders, the $\alpha_1\alpha_2$ components were well separated so no special precaution was taken to exclude the α_2 contribution. From these distributions, the respective α_1 slice scans were extracted. For 444 and 555, the slice scans only were recorded, no attempt being made to gather the $\Delta\omega, \Delta 2\theta$ distributions because of their low intensity.

As noted earlier in the text, the reflectivity distributions for the four orders are closely similar (Fig. 4*a*). They each show the same distribution of 'fragments'. There is, however, one unexpected feature. For 333, the reflectivity curve, and the corresponding $\Delta\omega, \Delta 2\theta$ distribution, show the existence of a peak that does not appear in any of the other three. The existence of an additional '333' fragment must therefore be excluded. It is clear, however, from the $\Delta\omega, \Delta 2\theta$ distribution in Fig. 5(*a*) and the 'film' profile in Fig. 5(*b*) (Mathieson & Stevenson, 1986*b*) that its Bragg angle (and hence spacing) corresponds exactly to that of a 333 reflection. It must therefore be associated with a 511 reflection and arise from twinning on a {111} plane. This feature, which is revealed only by the resolution capability of the $\Delta\omega, \Delta 2\theta$ and slice-scan technique, presents an example of a possible source of error – namely that, under such circumstances, a given cubic reflection, $h_1k_1l_1$, could involve a component of another reflection, $h_2k_2l_2$, where $h_1^2 + k_1^2 + l_1^2 = h_2^2 + k_2^2 + l_2^2$. Such an event would not be readily detected if only a normal profile was recorded (see Fig. 4*b*) and so it has the potential to introduce error in the estimate of intensity and hence of the structure factor.

In order to demonstrate conclusively that the origin of the extra peak in the 333 reflectivity distribution is as mentioned above, special scans of the type mentioned by Stevenson & Pain (1990), for studying twinning, were collected about the [111], [$\bar{1}$11], [1$\bar{1}$1] and [11$\bar{1}$] axes. These scans are essentially circles in the appropriate pole figures with a polar angle of 70.5°, and a special diffractometer control program has been written to perform such scans. The results clearly demonstrated the presence of twinning only about the [111] axis.

The slice-scan measurements on magnetite, which were made with the 'thin' source (size 40 μm) (Mathieson & Stevenson, 1984) and Ag $K\alpha_1$ radiation, revealed no unusual features but did demonstrate the resolution capability of the technique. Fig. 6 shows the results on the 404 reflection, namely a FWHM of 130″. Also shown is the calculated resolution function involving the source, the crystal size, the wavelength band and the detector slit, FWHM estimated as 45″.

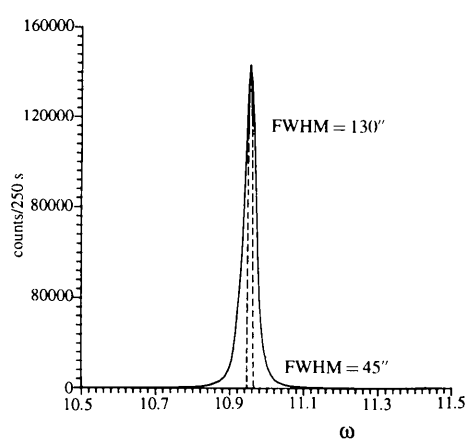

Fig. 6. Slice-scan distribution of the 404 reflection of magnetite with FWHM of 130″. The calculated resolution function (dashed curve) corresponding to the experiment components, namely the source size, the crystal size, the wavelength band and the detector aperture size, has a FWHM of 45″.

We are grateful to Dr R. M. Crenko of the Research and Development Centre, General Electric Company, Schenectady, NY 12301, USA, for crystals of cubic BN, to the late Dr R. C. Croft of CSIRO, Australia, for crystals of magnetite, and to Dr A. J. Morton of the Division of Materials Science and Technology, CSIRO, Australia, for advice on matters of twinning. We are also grateful to Dr U. W. Arndt of MRC, Cambridge, England, for invaluable comments on our original text.

References

BURBANK, R. D. (1964). *Acta Cryst.* **17**, 434–442.
CLARK, R. C. (1993). *Acta Cryst.* A**49**, 692–697.
DARWIN, C. G. (1922). *Philos. Mag.* **43**, 800–829.
DESTRO, R. & MARSH, R. E. (1993). *Acta Cryst.* A**49**, 183–190.
FURNAS, T C. (1957). *Single Crystal Orienter Instruction Manual.* General Electric Company, Milwaukee, USA.
International Tables for Crystallography (1992). Vol. C. *Mathematical, Physical and Chemical Tables*, edited by A. J. C. WILSON, pp. 530–536. Dordrecht: Kluwer Academic Publishers.

KEULEN, E. (1969). Doctoral thesis, Groningen Univ., The Netherlands.
MATHIESON, A. McL. (1968). *Rev. Sci. Instrum.* **39**, 1834–1837.
MATHIESON, A. McL. (1979). *Acta Cryst.* A**35**, 50–57.
MATHIESON, A. McL. (1982). *Acta Cryst.* A**38**, 378–387.
MATHIESON, A. McL. (1984). *J. Appl. Cryst.* **17**, 207–209.
MATHIESON, A. McL. (1985). *Acta Cryst.* A**41**, 309–316.
MATHIESON, A. McL. & STEVENSON, A. W. (1984). *Aust. J. Phys.* **37**, 657–665.
MATHIESON, A. McL. & STEVENSON, A. W. (1986*a*). *Acta Cryst.* A**42**, 223–230.
MATHIESON, A. McL. & STEVENSON, A. W. (1986*b*). *Acta Cryst.* A**42**, 435–441.
MATHIESON, A. McL. & STEVENSON, A. W. (1993). *Acta Cryst.* A**49**, 655–661.
ROBINSON, B. W. (1933). *Proc. R. Soc. London Ser. A*, **142**, 422–447.
ROBINSON, B. W. (1934). *Proc. R. Soc. London Ser. A*, **147**, 467–478.
SCHNEIDER, J. R. (1977). *Acta Cryst.* A**33**, 235–243.
STEVENSON, A. W. (1989). *Acta Cryst.* A**45**, 75–85.
STEVENSON, A. W. & PAIN, G. N. (1990). *Aust. J. Phys.* **43**, 793–799.
STOKES, A. R. (1948). *Proc. Phys. Soc. London*, A**61**, 382–391.

Acta Cryst. (1995). A**51**, 398–404

The *Ab Initio* Crystal Structure Solution of Proteins by Direct Methods. IV. The Use of the Partial Structure

BY CARMELO GIACOVAZZO

Dipartimento Geomineralogico, Università di Bari, Campus Universitario, Via Orabona 4, 70125 *Bari, Italy*

AND JAVIER GONZALEZ PLATAS

Departamento de Fisica Fundamental y Experimental, Universidad de La Laguna, E-38203 *La Laguna, Tenerife, Spain*

(*Received* 9 *May* 1994; *accepted* 5 *December* 1994)

Abstract

A probabilistic formula originally designed for small molecules, which allows the recovery of the complete from a partial structure [Giacovazzo (1983). *Acta Cryst.* A**39**, 685–692], is reconsidered. Experimental tests show that the formula is potentially able to estimate phases accurately provided 30–40% of the electron density is correctly located. The formula may be used for refining the phase values obtained by isomorphous derivative techniques as well as for extending the phasing process to a resolution higher than the derivative resolution.

Symbols and notation

Papers by Giacovazzo, Siliqi & Ralph (1994), Giacovazzo, Siliqi & Spagna (1994) and Giacovazzo, Siliqi & Zanotti (1995) are referred to as papers I, II and III, respectively.

The symbols and the notation are basically those described in paper III. Additional symbols are necessary here and they are listed below:

$F_{\pi,\mathbf{h}} = |F_{\pi,\mathbf{h}}| \exp(i\varphi_{\pi,\mathbf{h}})$ Structure factor of a partial structure. The subscript p is used in papers I–III, as well as in this paper, to indicated protein.

$[\sigma_2^3/\sigma_3^2]_\pi$ (Statistically equivalent) number of atoms of the partial structure for the primitive unit cell.

$[\sigma_2^3/\sigma_3^2]_q$ (Statistically equivalent) number of atoms of the difference structure obtained by subtracting the partial from the protein structure.

$E''_{\mathbf{h}}$ Structure factors of the protein structure pseudo-normalized with respect to the difference structure.

$E''_{\pi,\mathbf{h}}$ Structure factors of the partial structure pseudo-normalized with respect to the difference structure.

Introduction

According to the tangent formula (Karle & Hauptman, 1956),

$$\tan\theta_{\mathbf{h}} = \frac{\sum_{j=1}^{r} G_j \sin(\varphi_{\mathbf{k}_j} + \varphi_{\mathbf{h}-\mathbf{k}_j})}{\sum_{j=1}^{r} G_j \cos(\varphi_{\mathbf{k}_j} + \varphi_{\mathbf{h}-\mathbf{k}_j})} = \frac{T_{\mathbf{h}}}{B_{\mathbf{h}}}. \quad (1)$$

$\theta_{\mathbf{h}}$ is the most probable value of $\varphi_{\mathbf{h}}$. Its reliability depends on the concentration parameter

$$\alpha_{\mathbf{h}} = (T_{\mathbf{h}}^2 + B_{\mathbf{h}}^2)^{1/2}. \quad (2)$$

Relationship (1) has practically solved the phase problem for small molecules. Its application to two small proteins